Histol Histopathol (2023) 38: 1429-1441

Histology and Histopathology
From Cell Biology to Tissue Engineering

ORIGINAL ARTICLE Open Access

Hsa_circ_0070440 promotes lung adenocarcinoma progression by SLC7A11-mediated-ferroptosis

Yong Zhao[1], Qichen Cui[1], Jian Shen[1], Weihong Shen[2] and Yuan Weng[1]

[1]Department of Thoracic and Cardiac Surgery and [2]Department of Clinical Laboratory, Affiliated Hospital of Jiangnan University, Wuxi, Jiangsu, China

Summary. Background. Circular RNA (circRNA) has recently emerged as having a key role in cancer initiation and progression. A prior study exhibited that hsa_circ_0070440 (circ_0070440) was significantly up-regulated in lung cancer cells, but the role and molecular mechanism of circ_0070440 during lung adenocarcinoma (LUAD) development remain unclear.

Methods. Quantitative real-time polymerase chain reaction (qRT-PCR), Reverse transcription-PCR (RT-PCR), RNase R digestion, and Nuclear/cytoplasmic fractionation assay were employed to validate circ_0070440. Proliferation, apoptosis, viability, and ferrous iron level were measured by colony formation, 5-Ethynyl-2'-deoxyuridine (EdU), Annexin V-FITC/PI double staining, Cell Counting Kit-8 (CCK-8), and iron assay in LUAD cells. A xenograft mouse model was used for tumor growth *in vivo*. Western blot (WB) and immunohistochemistry (IHC) assays were utilized to determine the expression of solute carrier family 7 member 11 (SLC7A11), c-myc, and bcl-xL. The interactions between the circ_0070440/SLC7A11 axis and miR-485-5p were verified by RNA pull-down assay and dual-luciferase reporter assay.

Results. Circ_0070440 was significantly up-regulated in LUAD cells. Knockdown of circ_0070440 inhibited growth and promoted both apoptosis and ferroptosis of LUAD cells. Moreover, our results showed that circ_0070440 contributed to malignant progression and suppressed ferroptosis of LUAD by sponging miR-485-5p and upregulating SLC7A11 expression. Furthermore, circ_0070440 and SLC7A11 levels were up-regulated, and the miR-485-5p level was more down-regulated in the tumor tissues than in normal tissues of LUAD patients.

Conclusion. Circ_0070440 modulated LUAD malignant progression and ferroptosis via targeting SLC7A11, implying a significant role of the circ_0070440/miR-485-5p/SLC7A11 axis in the diagnosis and treatment of LUAD.

Key words: Lung adenocarcinoma, circ_0070440, miR-485-5p, SLC7A11

Introduction

GLOBOCAN 2020 estimated that lung cancer, with 2,206,771 new cases diagnosed and 1,796,144 deaths worldwide, accounted for 11.7% of the total cancer incidence and 18.0% of the total deaths (Sung et al., 2021). Lung adenocarcinoma (LUAD) is a kind of malignant tumor derived from bronchial mucosa glandular epithelium, consisting of about 50% of all lung cancers, and its frequency is increasing (Barta et al., 2019; Lambe et al., 2020). Despite extensive research and progress, the treatment of LUAD is still inadequate and needs further improvement (Succony et al., 2021). Therefore, it is extremely urgent to find new molecular targets to develop more effective LUAD treatment strategies.

CircRNA is a new kind of endogenous non-coding RNA molecule with a stable closed circular structure formed by reverse splicing. Unlike traditional linear RNA (containing 5' and 3' ends), circRNA is not affected by RNA exonucleases, is more stable in expression, and is less susceptible to degradation (Ebesen et al., 2016). CircRNAs have the characteristics of high stability, high conservation among species, and tissue specificity, and have been regarded as potential molecular biomarkers in various disorders (Bing et al., 2018). As powerful effect mediators of diverse biological processes, such as proliferation, death, metastasis, and metabolism in cancer, circRNA regulates gene expression through a variety of molecular mechanisms, including serving as the sponge for microRNA (miRNA) and protein adsorbers (Hansen et al., 2013; Bing et al., 2018; Tao et al., 2021). For example, circRHOT1 restrained breast cancer cell

Corresponding Author: Yuan Weng, MM, Department of Thoracic and Cardiac Surgery, Affiliated Hospital of Jiangnan University (South Branch), No. 1000 Hefeng Road, Binhu District, Wuxi City, Jiangsu Province, 214122, PR China. e-mail: wengy123456@126.com
www.hh.um.es. DOI: 10.14670/HH-18-597

apoptosis and ferroptosis, but contributed to metastasis by interacting with miR-106a-5p to elevate STAT3 level (Zhang et al., 2021a). As shown in investigations, circDLC1, a downstream target of KIAA1429, could repress liver cancer proliferation and metastasis via the HuR/MMP1 axis (Liu et al., 2021). Furthermore, it was found that high expression of ciRS-7 was associated with poor prognosis of RCC, and nanoparticles including si-ciRS-7 effectively suppressed growth and metastasis of RCC, which provides a new idea for RCC gene therapy (Mao et al., 2021). Therefore, circRNA might become a promising biomarker for LUAD diagnosis and treatment targets. Previous analyses have indicated that hsa_circ_0070440 (circ_0070440) is a novel circRNA that was up-regulated in lung cancer cells (Zhang et al., 2020), but its role and underlying mechanism in LUAD remain unknown.

In recent years, ferroptosis, a form of programmed cell death triggered by the accumulation of iron-dependent lipid reactive oxygen species, has played an important role in cancer (Koppula et al., 2021). Ferroptosis is due to the inactivation of GPX4, which leads to the accumulation of iron-dependent lipid peroxides in cells and results in cell death (Zheng and Conrad, 2020). Solute carrier family 7 member 11 (SLC7A11), also named xCT, which mediates cystine uptake, plays a key role in inhibiting oxidative reactions and maintaining cell survival under oxidative stress (Koppula et al., 2021). In the recent literature, SLC7A11 has been recognized as a promising target in lung cancer treatment. SLC7A11 was up-regulated in lung cancer patients and cells, and knockdown of SLC7A11 was able to constrain the cell metabolic requirements, such as consumption of cystine and the release of glutamate, and promoted ferroptosis to inhibit lung cancer progression (Ji et al., 2018; Hu et al., 2020; Yuan et al., 2020; Ma et al., 2021; Zhang et al., 2021b). Interestingly, recent studies have uncovered that circRNA also played a vital role in regulating ferroptosis. Nevertheless, there is a lacking of information on the effects of circ_0070440 on ferroptosis.

In this study, we found that circ_0070440 was up-regulated in LUAD cells and tissues. Notably, circ_0070440 facilitated LUAD malignant progression and inhibited ferroptosis by sponging miR-485-5p to increase SLC7A11 expression, implying that the circ_0070440/miR-485-5p/SLC7A11 axis might allow for a better understanding of the development of LUAC.

Materials and methods

Cell Culture

Human LUAD cells HCC827 (C6298; Beyotime, Shanghai, China) and Human bronchial epithelioid cells 16HBE (CL-0249; Procell, Wuhan, China) were cultured in RPMI-1640 medium (01-100-1A; Bioind, Israel) at 37°C with 5% CO_2. Human LUAD cells A549 (C6053; Beyotime) and Human Embryonic Kidney Cells 293T (C6008; Beyotime) were maintained in DMEM medium (01-056-1A; Bioind) at 37°C with 5% CO_2. All mediums were added with 1×penicillin/streptomycin (C0222; Beyotime) and 10% FBS (C0232; Beyotime).

Cell transfection

The lentiviral vector pLKO.1-puro-sh-circ_0070440 (sh-circ_0070440) containing shRNA of targeting circ_0070440 junction sites and pLKO.1-puro-sh-NC vector (sh-NC) were constructed and then packaged into lentivirus by Biofeng (Shanghai, China). The CMV/EGFP/Blasticidin vector containing miR-485-5p, miR-NC, miR-485-5p inhibitor (anti-miR-485-5p), NC inhibitor (anti-NC), and a pcDNA3.1-SLC7A11 vector containing full-length SLC7A11 were acquired from Songon (Shanghai, China). The above vectors and oligonucleotides were transfected into A549 and HCC827 cells using Lipofectamine 3000 (L3000008; Invitrogen, Carlsbad, CA, USA).

RNA, DNA purification, and reverse transcription

Total RNA Extraction Kit (R1200; Solarbio, Beijing, China) and Universal Genomic DNA Extraction Kit (D2100; Solarbio) were respectively used for extracting RNA and genomic DNA (gDNA). First Strand cDNA Synthesis Kit (K621; Thermo Fisher Scientific, Rockville, MD, USA) and miRNA First Strand cDNA Synthesis Kit (B532453; Songon) were employed to reverse transcription of RNA into cDNA.

Quantitative real-time polymerase chain reaction (qRT-PCR)

2X SYBR Green Abstart PCR Mix (B110031; Songon) and MicroRNAs qPCR Kit (B532461; Songon) were utilized to assess the level of circ_0070440, SLC7A11 mRNA, miR-345-5p, and miR-485-5p. U6 or β-actin was employed as the internal reference. The relative expression level with respect to the control sample was calculated via the $2^{-\Delta\Delta CT}$ method. The primers are provided in Table 1.

Agarose gel electrophoresis

The 2×Taq Master Mix (P111-01; Vazyme, Nanjing, China) was used to detect the expression of circ_0070440 in cDNA and gDNA. PCR products were separated and confirmed by 3% agarose gel electrophoresis and 50 bp Ladder DNA Marker (MD111-01; Biomed, Guangzhou, China).

RNase R digestion

10 μg RNAs of cells were extracted and then performed with 2U RNase R (M1228-500; Biovision, Milpitas, CA, USA) for 1 hour at 37°C. The levels of circ_0070440 and β-actin were quantified by qRT-PCR.

Nuclear/cytoplasmic fractionation

Nuclear and cytoplasmic RNAs of cells were isolated using PARIS™ Kit (AM1921; Invitrogen). After purification and DNase I (D8071; Solarbio) treatment, nuclear and cytoplasmic RNAs were reverse-transcribed into cDNAs. qRT-PCR was employed to monitor the expression level of circ_0070440, β-actin, and U6.

Colony formation assay

Cells (500) were seeded and cultured in 6-well plates for 10 days. The colonies were fixed and stained with Paraformaldehyde (4%; P1110; Solarbio) and Crystal violet solution (0.1%; G1064; Solarbio), and then were quantified via Image-Pro Plus software.

EdU assay

Cells (5×10^3) were inoculated in 96-well plates for 24 hours and then were treated and fixed with Yefluor 488 EdU Imaging Kits (40275ES60; YEASEN, Shanghai, China) and Paraformaldehyde. Images were visualized using an Olympus FSX100 microscope (Olympus, Japan).

Cell apoptosis assay

Cells (5×10^5) were resuspended and stained with Annexin V-FITC/PI Apoptosis Detection Kit (40302ES20; YEASEN), and the samples were examined by flow cytometry within 1 hour.

Cell viability assay

Cells (5×10^5) were inoculated in 96-well plates and treated with DMSO (Dimethyl sulfoxide; D8371; Solarbio), 2 μM/mL Ferrostatin-1 (Fer-1; S7243; Selleck Chemicals, Houston, TX, USA) or 5 μM/mL Erastin (S7242; Selleck Chemicals) for 24 hours. The OD450 was measured 1 hour after adding CCK-8 Kit (40203ES60; YEASEN) into cells.

Table 1. Primer sequences used for PCR.

Name		Primers for PCR (5'-3')
hsa_circ_0070440	Forward	GGTAACGTGAAGGTGGTGGA
	Reverse	CGCTGCTTTACTTTGCCTGA
SLC7A11	Forward	TCTCCAAAGGAGGTTACCTGC
	Reverse	AGACTCCCCTCAGTAAAGTGAC
miR-485-5p	Forward	GATGAGAGAGGCTGGCCGTG
	Reverse	CTCAACTGGTGTCGTGGAGTC
miR-345-5p	Forward	GATTCCAGGCTGACTCCTAGT
	Reverse	CTCAACTGGTGTCGTGGAGTC
U6	Forward	CTTCGGCAGCACATATACT
	Reverse	AAAATATGGAACGCTTCACG
β-actin	Forward	CTTCGCGGGCGACGAT
	Reverse	CCACATAGGAATCCTTCTGACC

GSH assay

Cells (6×10^3) were cultured in 96-well plates until the next day. GSH levels were estimated using the GSH-Glo Glutathione Assay kit (V6911; Promega, Madison, WI, USA) as previously described (Zhang et al., 2021b).

Iron assay

Ferrous iron (Fe^{2+}) levels of cells (2×10^6) were measured by using Iron Assay Kit (MAK025; Sigma-Aldrich, Louis, MO, USA) as previously described (Wang et al., 2019).

Western blot

Total protein was extracted via Total Protein Extraction Kit (BC3710; Solarbio), separated by 10% sodium dodecyl sulfate-polyacrylamide gel electrophoresis (P1203; Solarbio), and subsequently electrotransferred onto polyvinylidene fluoride membranes (0.22 μm; YA1700; Solarbio). Membranes were then blocked with 5% NON-Fat Powdered Milk (D8340; Solarbio) for 1 hour at room temperature and then incubated with primary antibodies against SLC7A11 (Anti-xCT; 1:2000; ab37185; Abcam, Cambridge, MA, USA), c-myc (Anti-c-Myc; 1:1000; ab32072; Abcam), bcl-xl (Bcl-XL Polyclonal Antibody; 1:1000; 26967-1-AP; Abcam), and β-actin (beta Actin Antibody; 1:4000; MA5-15739; Invitrogen) overnight at 4°C. Next, the membranes were incubated with Goat Anti-Rabbit IgG H&L (HRP) antibody (1:10000; ab6721; Abcam), and then protein signals were measured by High Sensitivity ECL Substrate Kit (ab133406; Abcam).

Mouse xenograft model

The animal study procedures received the approval of the Animal Care Committee of the Affiliated Hospital of Jiangnan University (South Branch). A549 cells (3×10^6) transfected with sh-circ_0070440 or sh-NC were resuspended in 100 μL PBS and subcutaneously injected into the flank area of the BALB/c Nude (n=5 in each group; 401; Vital River, Beijing, China). The tumor volume was assessed every 5 days and was calculated based on the equation: $\text{length}\times\text{width}^2\times0.5$. After 30 days, the mice were sacrificed and the tumor was dissected for the following IHC analysis.

IHC assay

Excised tumor samples were fixed, dehydrated, embedded in paraffin, and cut into 4 μm thick sections. The primary antibodies SLC7A11 (Anti-xCT; 1:500; ab37185; Abcam), c-myc (Anti-c-Myc; 1:100; ab32072; Abcam), bcl-xl (Bcl-XL Polyclonal Antibody; 1:200; 26967-1-AP; Abcam), second antibody Goat Anti-

Rabbit IgG H&L (HRP) antibody (1:10000; ab6721; Abcam), and IHC Detection Kit (E-IR-R213; Elabscience, Wuhan, China) were used to monitor the expression of SLC7A11, c-myc, and bcl-xl.

RNA pull-down assay

As previously described (Chen et al., 2017), cell lysates were incubated with a biotin-labeled probe against circ_0070440 junction site (circ_0070440 probe; Songon) and negative probe (NC probe; Songon). Biotin-coupled complexes were pulled down with Streptavidin immunomagnetic beads (D110557; Songon) and used for the analysis of miR-345-5p and miR-485-5p by qRT-PCR.

Dual-luciferase reporter assay

The pmirGLO luciferase vector containing wild type (wt) and mutated (mut) circ_0070440 or SLC7A11-3' UTR sequence (wt-circ_0070440, mut-circ_0070440, wt-SLC7A11-3' UTR, mut-SLC7A11-3' UTR) were constructed by Genepharma (Shanghai, China). The above vectors were co-transfected with miR-485-5p or miR-NC into cells using Lipofectamine 3000 (L3000008; Invitrogen) for 48 hours and the luciferase activity was evaluated via Dual Luciferase Reporter Gene Assay Kit (E608001; Songon).

Clinical sample

Fresh nearby normal tissues and LUAD tumor tissue samples came from LUAD patients (n=42) who had received surgery. Tissue samples were subjected to qRT-PCR, WB, and IHC analyses to measure the expression of circ_0070440, miR-485-5p, and SLC7A11. This experiment was approved by the Ethics Committee of the Affiliated Hospital of Jiangnan University (South Branch). All participants received written informed consent.

Statistical analysis

All statistical analyses were performed with GraphPad Prism 9 software. Data are expressed as means±standard deviations (SD). Differences among groups were analyzed by Student's *t*-test (two groups) or one-way analysis of variance (ANOVA) with Tukey's post hoc test. $P<0.05$ was considered statistically significant.

Results

The characterization of circ_0070440 in LUAD cells

First, we found that circ_0070440 level was conspicuously up-regulated in LUAD cells (A549 and HCC827) in contrast to normal cells (16HBE) by qRT-PCR (Fig. 1A). By mapping the sequences of circ_0070440 to the human reference genome (GRCh37.87/hg19, chr4:89941610-89950800[-]), we indicated that circ_0070440 consists of exons 2 and 3, derived from FAM13A, and back-splicing junction sites of circ_0070440 were proved by Sanger sequencing (Fig. 1B). Next, the cyclization of

circ_0070440 was validated by PCR analysis and RNase R digestion assay. PCR and agarose gel electrophoresis results indicated that divergent primers of circ_0070440 amplified products from cDNA but not from gDNA (Fig. 1C). RNase R digestion assay suggested that circ_0070440 was resistant to RNAse R treatment, whereas β-actin mRNA was easily degraded (Fig. 1D,E). Moreover, Nuclear/Cytoplasmic fractionation followed by qRT-PCR analysis demonstrated that circ_0070440 was preferentially located in the cytoplasm of A549 and HCC827 cells (Fig. 1F,G). The knockdown efficiency of circ_0070440 was verified in A549 and HCC827 cells (Fig. 1H), and the data showed no regulatory effect of circ_0070440 on FAM13A expression (Fig. 1I). These results suggested that the role of circ_0070440 maybe benefited from its biological stability.

Circ_0070440 facilitated proliferation and inhibited apoptosis and ferroptosis in LUAD cells

We used loss-of-function assays to uncover the function of circ_0070440. Colony formation and EdU assay results manifested that the downregulation of circ_0070440 dramatically restrained A549 and HCC827 cell proliferation (Fig. 2A,B). Moreover, circ_0070440 silencing markedly boosted cell apoptosis based on Annexin V-FITC/PI assay (Fig. 2C). We next examined the role of circ_0070440 in ferroptosis. Knowdown of circ_0070440 markedly reinforced the Erastin (ferroptosis inducer) -induced viability suppression, this process was reversed by the ferrostatin-1 (Fer-1, ferroptosis inhibitor) in A549 and HCC827 cell, indicating that the downregulation of circ_0070440 inhibited cell viability in a ferroptosis-dependent manner (Fig. 2D,E). Again, circ_0070440 knockdown decreased the GSH level and increased the Fe^{2+} level (Fig. 2F,G). Previous studies have suggested that SLC7A11 acted as a suppressor of ferroptosis in lung cancer. We detected the protein level of SLC7A11 and its downstream molecules c-myc and bcl-xl (Ji et al., 2028). Intriguingly, silencing circ_0070440 significantly reduced the protein levels of SLC7A11, c-myc, and bcl-xl in A549 and HCC827 cells (Fig. 2H,I). These results demonstrated that circ_0070440 enhanced the malignant progression of LUAD cells *in vitro*.

Circ_0070440 enhanced tumor growth in vivo

A549 cells transfected with sh-NC or sh-circ_0070440 were inoculated into nude mice, which indicated that sh-circ_0070440 notably constrained the growth of tumors more than sh-NC *in vivo* (Fig. 3A,B).

Subcutaneous tumor tissues were sectioned and stained with IHC. Results revealed that a reduction in circ_0070440 also suppressed the level of SLC7A11, c-myc, and bcl-xl in tumor tissue (Fig. 3C). Taken together, these results disclosed that circ_0070440 might contribute to LUAD growth *in vivo*.

Circ_0070440 modulated LUAD cell malignant progression by targeting SLC7A11

To understand if circ_0070440 induced malignant behaviors by modulating the expression of SLC7A11, we transfected circ_0070440-reduced A549 and HCC827 cells with a construct expressing SLC7A11 or a control vector. Consistent with previous studies, the SLC7A11 level was distinctly increased in A549 and HCC827 cells compared to 16HBE cells (Fig. 4A). The successful establishment of the SLC7A11 overexpression vector was shown by qRT-PCR after transfecting A549 and HCC827 cells (Fig. 4B). Overexpression of SLC7A11 partially recuperated circ_0070440 knockdown-induced suppression of cell proliferation (Fig. 4C,D) and promotion of cell apoptosis in A549 and HCC827 cells (Fig. 4E). Moreover, the reexpression of SLC7A11 retarded circ_0070440 depletion-inhibited cell viability in Erastin-treated A549 and HCC827 cells (Fig. 4F,G). Consistently, circ_0070440 depletion-induced decrease in GSH level

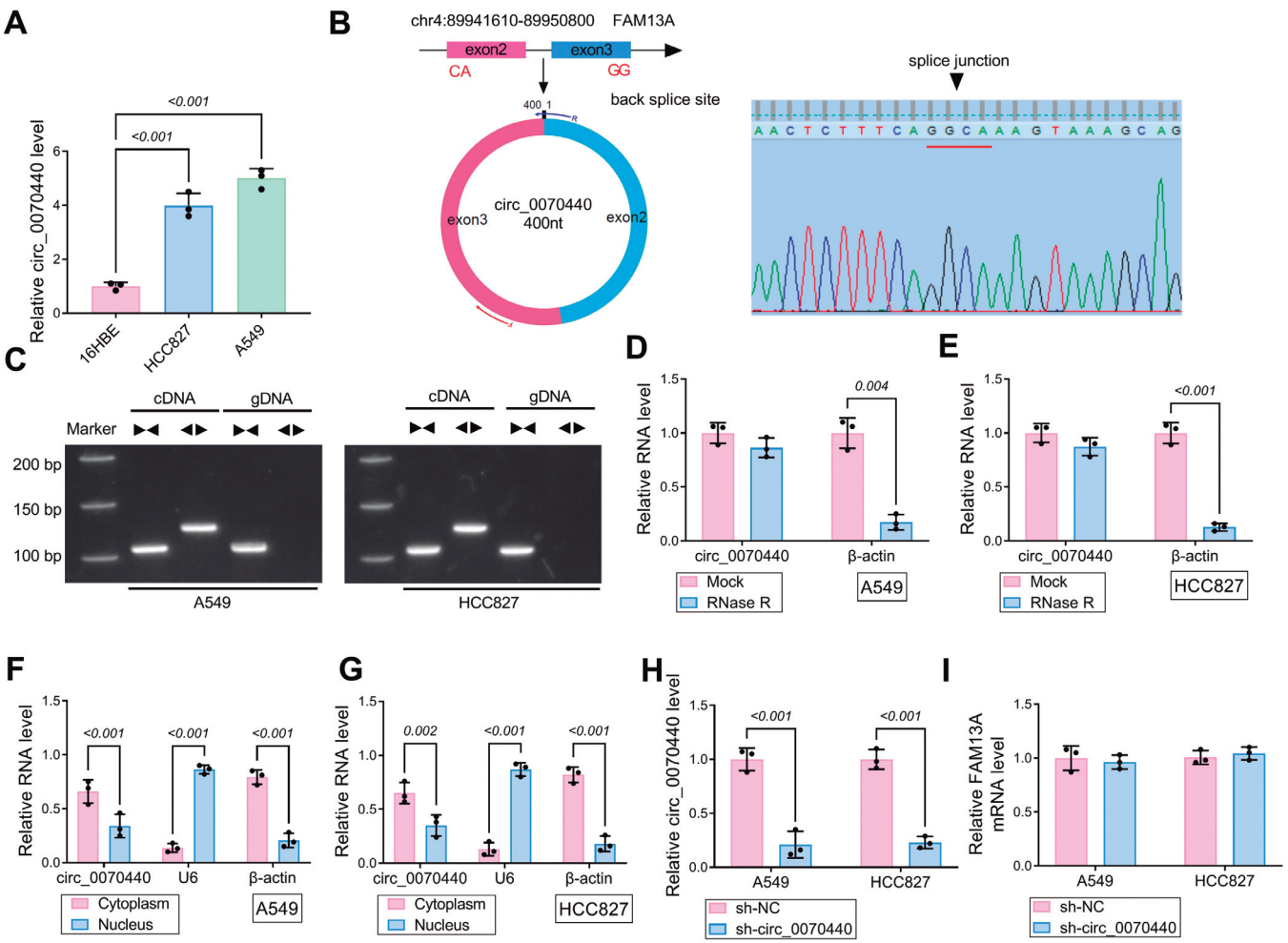

Fig. 1. A. Expression and characterization of circ_0070440 in LUAD cells. circ_0070440 level in LUAD cells (A549 and HCC827) and normal cells (THLE-2) using qRT-PCR. **B.** Circ_0070440 was back-spliced by exons 2 and 3 of the FAM13A gene and validated by Sanger sequencing. PCR primers used to specifically detect circ_0070440 by qRT-PCR were indicated by F (Forward primer) and R (Reward primer). **C.** RT-PCR or PCR assays for the detection of circ_0070440 using divergent and convergent primers from cDNA or gDNA of the A549 and HCC827 cells. **D, E.** qRT-PCR for the RNA level of circ_0070440 and β-actin with RNase R digestion in A549 and HCC827 cells. **F, G.** qRT-PCR for the distribution of circ_0070440, β-actin, and U6 in the cytoplasmic and nuclear fractions of A549 and HCC827 cells, β-actin and U6 were applied as positive controls in the cytoplasm and nucleus, respectively. **H, I.** qRT-PCR for the expression level of circ_0070440 and FAM13A in A549 and HCC827 cells transfected with sh-circ_0070440 or sh-NC. Data represent mean±SD.

(Fig. 4H) and increase in Fe^{2+} level (Fig. 4I) were also rescued by overexpression of SLC7A11. Further examination of protein levels by WB for A549 and HCC827 cells manifested that circ_0070440-depleted cells had reduced SLC7A11, c-myc, and bcl-xl protein levels compared with control, but this decrease was markedly recovered upon overexpression of SLC7A11 (Fig. 4J,K). To sum up, our results implicated that the downregulation of circ_0070440 constrained LUAD progression partially through repressing SLC7A11 and facilitating ferroptosis.

Circ_0070440 directly interacted with miR-485-5p to regulate the expression of SLC7A11 in LUAD cells

To better understand the molecular mechanisms underlying circ_0070440-regulated SLC7A11 expression in LUAD, the starbase (https://starbase.sysu.edu.cn) (Li et al., 2014) and circbank (http://www.circbank.cn/index.html) (Liu et al., 2019)

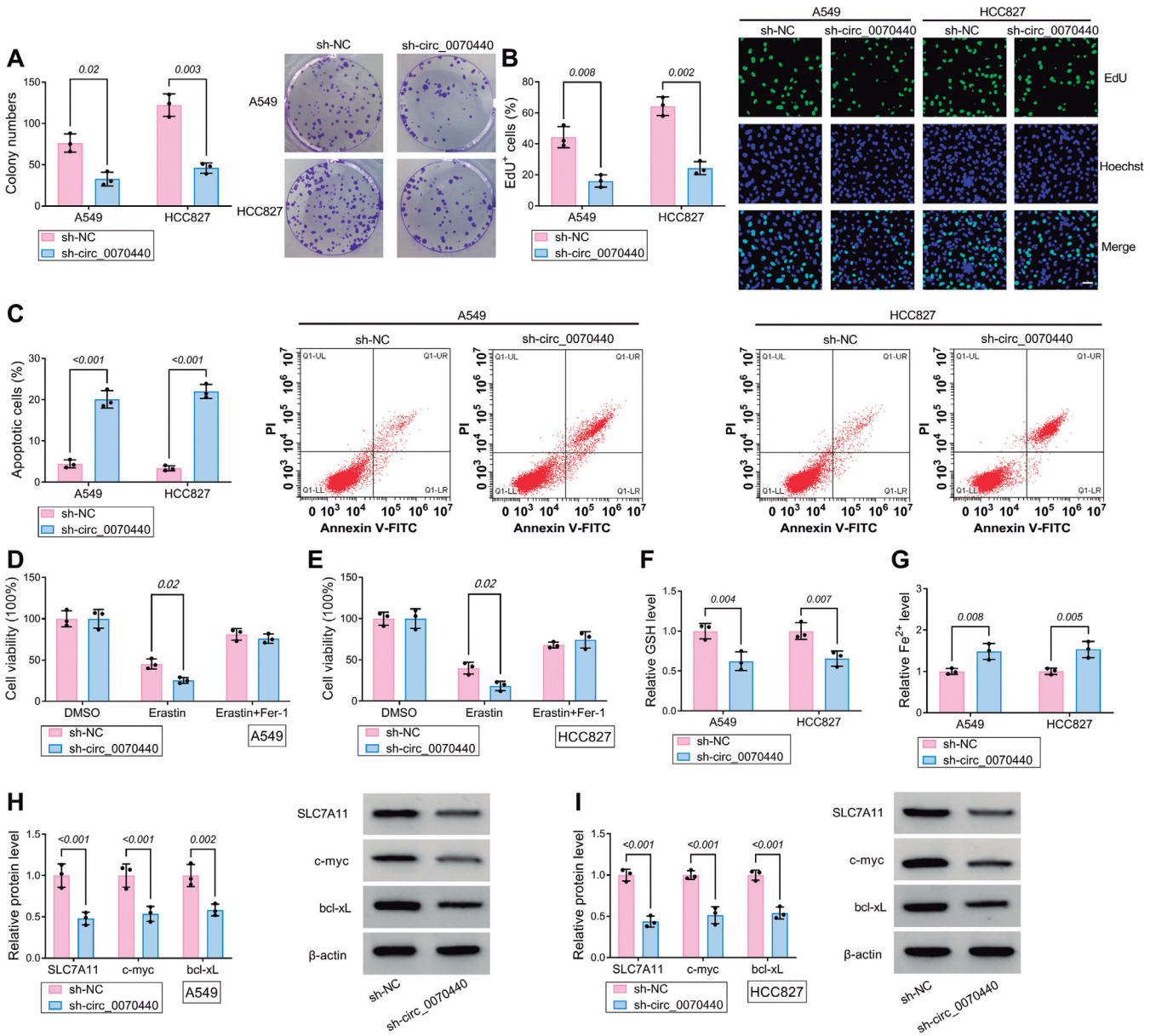

Fig. 2. Circ_0070440 contributed to LUAD cell proliferation and inhibited apoptosis and ferroptosis. **A, B.** Cell proliferation and apoptosis analysis **(C)** of A549 and HCC827 cells with silencing circ_0070440. **D, E.** Cell viability was measured after treatment with Erastin or Erastin and Fer-1 in circ_0070440-depleted A549 and HCC827 cells. **F.** GSH level and Fe^{2+} level **(G)** were assessed in circ_0070440-depleted A549 and HCC827 cells. **H, I.** WB analysis of SLC7A11, c-myc, and bcl-xl protein levels in A549 and HCC827 cells stably transfected with sh-circ_0070440 or sh-NC. Data represent mean±SD. Scale bars: 50 μm.

databases were utilized to predict the potential miRNAs that interacted with both circ_0070440 and SLC7A11 3'UTR. There were four candidate miRNAs (miR-421, miR-3064-5p, miR-345-5p, and miR-485-5p) containing common binding sites for circ_0070440 and SLC7A11 3'UTR (Fig. 5A). We found that miR-485-5p (Mou and Liu, 2016; Li et al., 2020) and miR-345-5p (Zhou et al., 2021) were down-regulated in LUAD and played a role in cancer suppression, and they were selected for subsequent studies. RNA pull-down results showed that the amount of miR-485-5p pulled down by the circ_0070440 probe was significantly more than that by the NC probe, indicating the existence of the binding site between circ_0070440 and miR-485-5p (Fig. 5B,C). The miR-485-5p level was significantly down-regulated in A549 and HCC827 cells compared to 16HBE cells by qRT-PCR (Fig. 5D). The wild type (wt) and mutated (mut) circ_0070440 or SLC7A11-3' UTR sequence (wt-circ_0070440, mut-circ_0070440, wt-SLC7A11-3' UTR, mut-SLC7A11-3' UTR) were inserted into pmirGLO luciferase reporter (Fig. 5E). The successful establishment of the miR-485-5p overexpression vector was shown by qRT-PCR after transfecting A549 and HCC827 cells (Fig. 5F). Luciferase activity assay showed that miR-485-5p overexpression markedly decreased the luciferase activity of wt-circ_0070440 reporter vector compared to the miR-NC, not mut-circ_0070440 reporter vector in A549 and HCC827 cells (Fig. 5G,H). As displayed in Figure 5I and Figure 5H, miR-485-5p efficiently decreased the luciferase activity of wt-SLC7A11-3' UTR reporter vector but not that of wt-SLC7A11-3' UTR reporter vector. QRT-PCR showed that miR-485-5p expression was increased in circ_0070440-reduced A549 and HCC827 cells, compared with the sh-NC groups (Fig. 5K). The protein level of SLC7A11 was effectively reduced by miR-485-5p (Fig. 5L). To investigate the potential functions of the circ_0070440/miR-485-5p axis on SLC7A11 expression, we successfully established the anti-miR-485-5p expression vector in A549 and HCC827 cells (Fig. 5M). It was consistent with our hypothesis that circ_0070440 knockdown reduced expression of SLC7A11 was enhanced by anti-miR-485-5p in A549 and HCC827 cells (Fig. 5N).

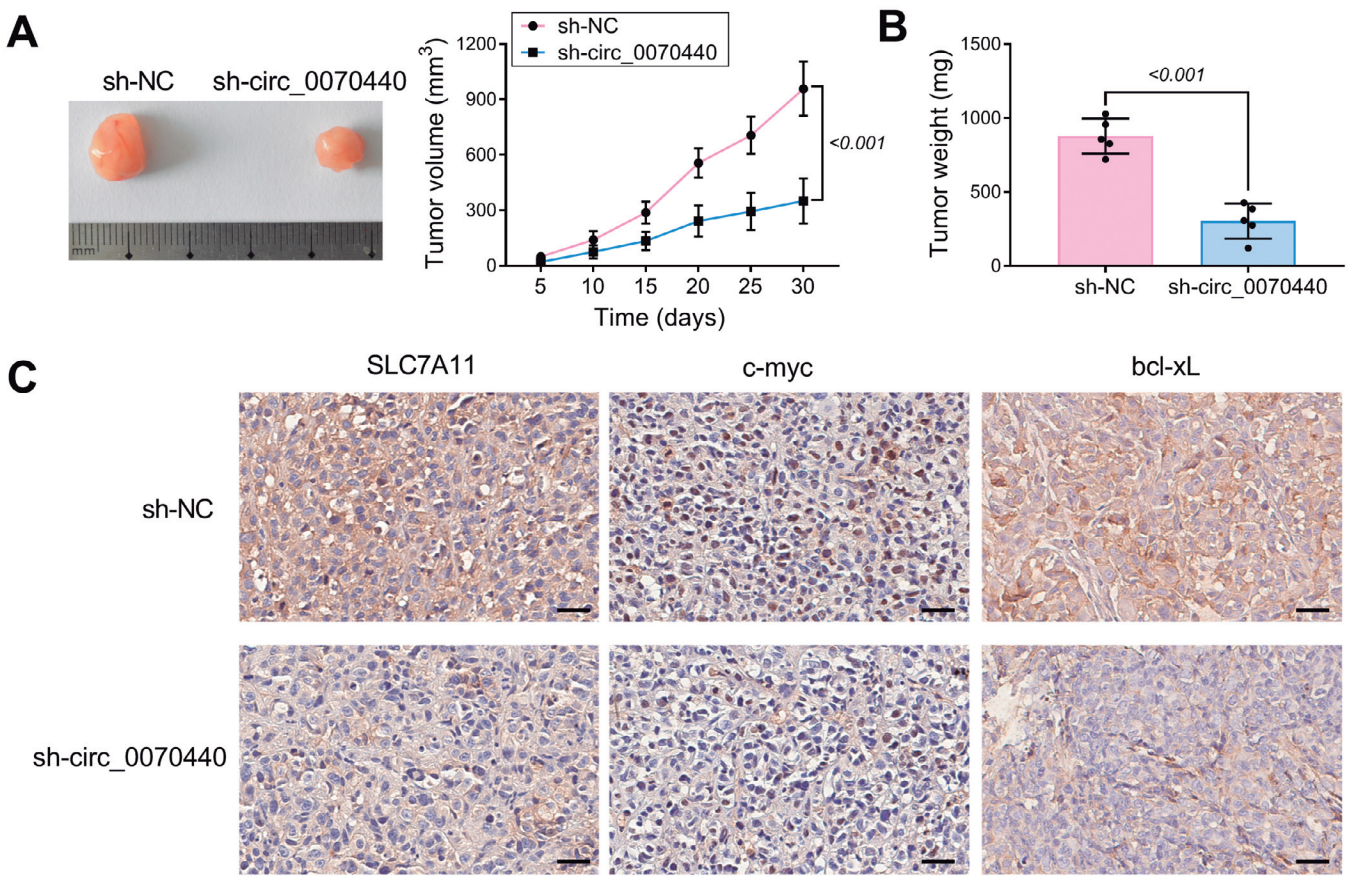

Fig. 3. Circ_0070440 promoted LUAD tumor growth *in vivo*. The volume **(A)** and weight **(B)** of subcutaneous xenograft tumors of A549 cells isolated from nude mice. **C.** IHC analysis of the SLC7A11, c-myc, and bcl-xl protein levels in subcutaneous xenograft tumors. Data represent mean±SD. Scale bars: 100 μm.

miR-485-5p mediated circ_0070440-dependent LUAD cell malignant progression

Next, we further investigated the role of miR-485-5p on circ_0070440-modulated LUAD cell malignant progression. Results showed that miR-485-5p knockdown rescued sh-circ_0070440-mediated suppression for proliferation (Fig. 6A,B) and promotion of cell apoptosis (Fig. 6C). In addition, the addition of anti-miR-485-5p relieved circ_0070440 depletion-induced cell viability inhibition in Erastin-induced A549 and HCC827 cells (Fig. 6D,E). Conspicuously, the

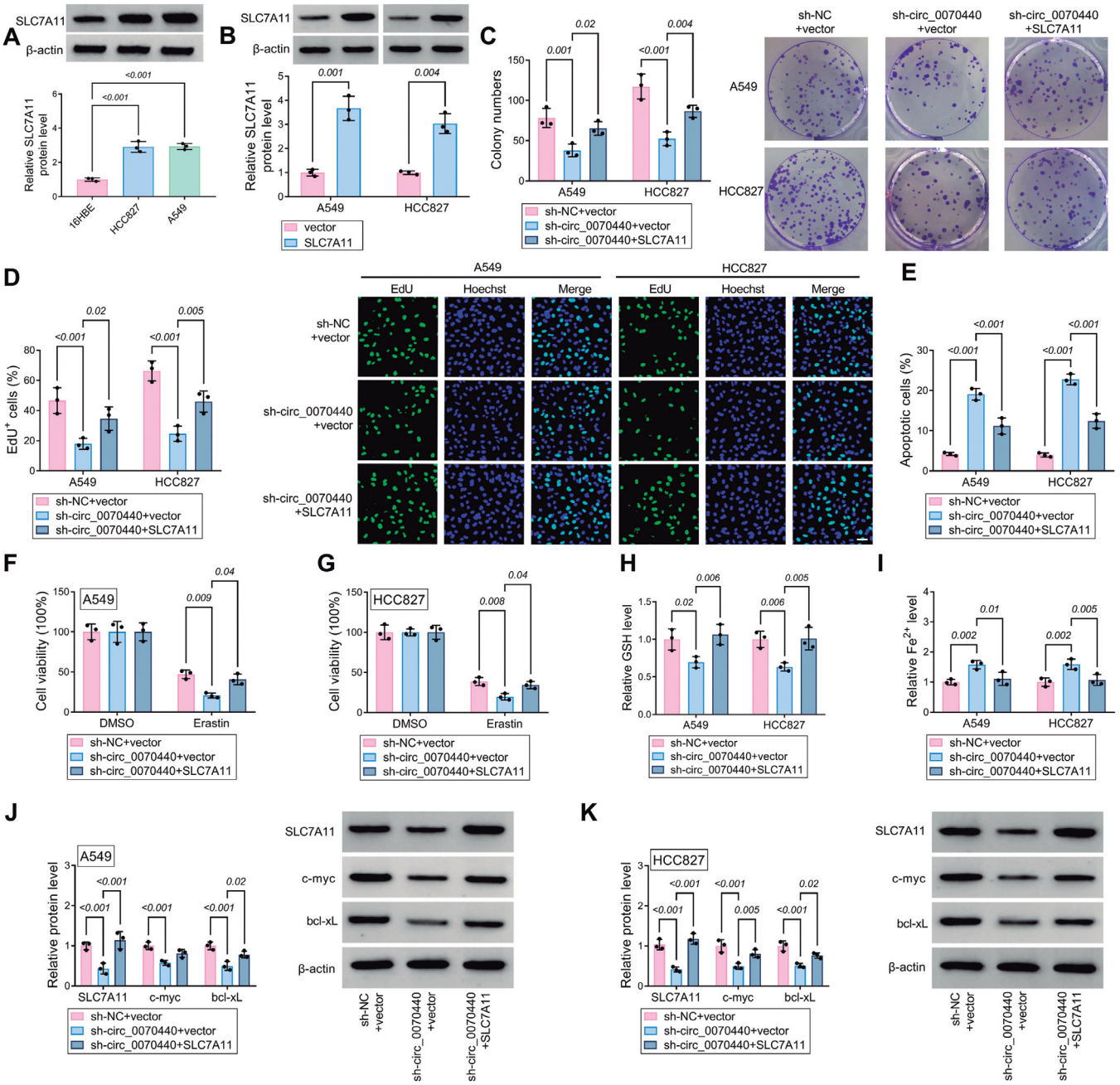

Fig. 4. Circ_0070440 contributed to cell progression by targeting SLC7A11. **A.** The levels of SLC7A11 protein in LUAD cells (A549 and HCC827) and normal cells (THLE-2). **B.** Expression levels of SLC7A11 protein in A549 and HCC827 cells transfected with pcDNA3.1-SLC7A11 (SLC7A11) or pcDNA3.1 (vector). **C, D.** Cell proliferation and apoptosis assay **(E)** for A549 and HCC827 cells with circ_0070440 knockdown and SLC7A11 overexpression. **F, G.** Cell viability of Erastin-treated, GSH level **(H)**, Fe^{2+} level **(I)**, and protein levels **(J, K)** of SLC7A11, c-myc, and bcl-xl were evaluated in A549 and HCC827 cells with circ_0070440 knockdown and SLC7A11 overexpression. Data represent mean±SD. Scale bars: 50 μm.

knockdown of circ_0070440 resulted in an evident decrease in GSH level (Fig. 6F) and an increase in Fe^{2+} level (Fig. 6G), which was significantly relieved by the addition of anti-miR-485-5p. Moreover, anti-miR-485-5p significantly attenuated the suppression effects of sh-circ_0070440 on the expression of c-myc and bcl-xl (Fig. 6H,I). These results proved that circ_0070440 can serve as a sponge for miR-485-5p to regulate SLC7A11 and promote cell malignant progression in LUAD cells

Expression of circ_0070440, miR-485-5p, and SLC7A11 in LUAD tissues.

We next measured the expression of circ_0070440, miR-485-5p, and SLC7A11 in 42 sets of paired LUAD and normal adjacent tissues. qRT-PCR data presented

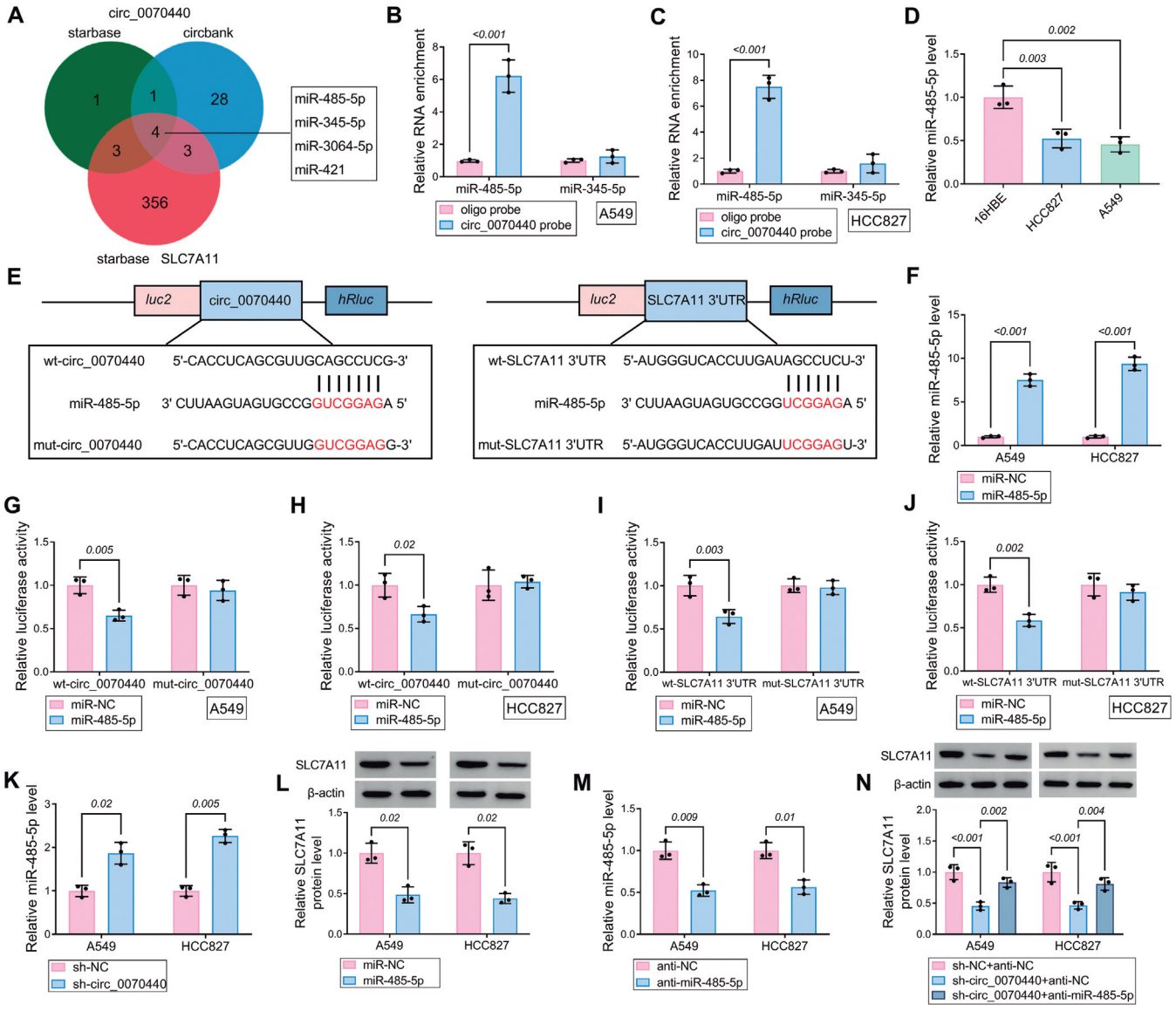

Fig. 5. Circ_0070440 targeted miR-485-5p to regulate SLC7A11 level in LUAD cells. **A.** Venn diagram showing the potential miRNAs that interacted with both circ_0070440 and SLC7A11 3'UTR by the intersection of the starbase and circbank databases. **B, C.** The interaction of circ_0070440 and miR-485-5p was identified by RNA-pull down assay. **D.** The levels of miR-485-5p in LUAD cells (A549 and HCC827) and normal cells (THLE-2) via qRT-PCR. **E.** Schematic drawing showing the sequence of wild-type (wt) and mutant (mut) circ_0070440 and SLC7A11 3'UTR. **F.** Expression levels of miR-485-5p in A549 and HCC827 cells transfected with miR-485-5p or miR-NC. **G-J.** Luciferase reporter activity of circ_0070440 and SLC7A11 3'UTR in A549 and HCC827 cells co-transfected with miR-485-5p or miR-NC. **K.** Expression levels of miR-485-5p in A549 and HCC827 cells transfected with sh-circ_0070440 or sh-NC. **L.** Expression levels of SLC7A11 protein in A549 and HCC827 cells transfected with miR-485-5p or miR-NC. **M.** Expression levels of miR-485-5p in A549 and HCC827 cells transfected with anti-miR-485-5p or anti-NC. **N.** Expression levels of SLC7A11 protein in A549 and HCC827 cells with circ_0070440 knockdown and miR-485-5p knockdown. Data represent mean±SD.

that circ_0070440 (Fig. 7A) and SLC7A11 (Fig. 7C) were highly expressed while miR-485-5p (Fig. 7B) was weakly expressed in LUAD in comparison with normal adjacent tissues. The protein level of SLC7A11 was also remarkably augmented in tumor tissues by IHC (Fig. 7D) and WB (Fig. 7E). Pearson correlation analysis demonstrated a positive correlation between circ_0070440 and SLC7A11 level (Fig. 7F), while both circ_0070440 (Fig. 7G) and SLC7A11 (Fig. 7H) level were negatively correlated with miR-485-5p level. These results showed correlations between circ_0070440, miR-485-5p, and SLC7A11 levels, and also supported their potential role in LUAD progress.

Discussion

To date, ferroptosis has been proven to be regulated by a variety of factors, thereby regulating cancer progression. More recently, some researchers have presented that ncRNAs might serve crucial roles in

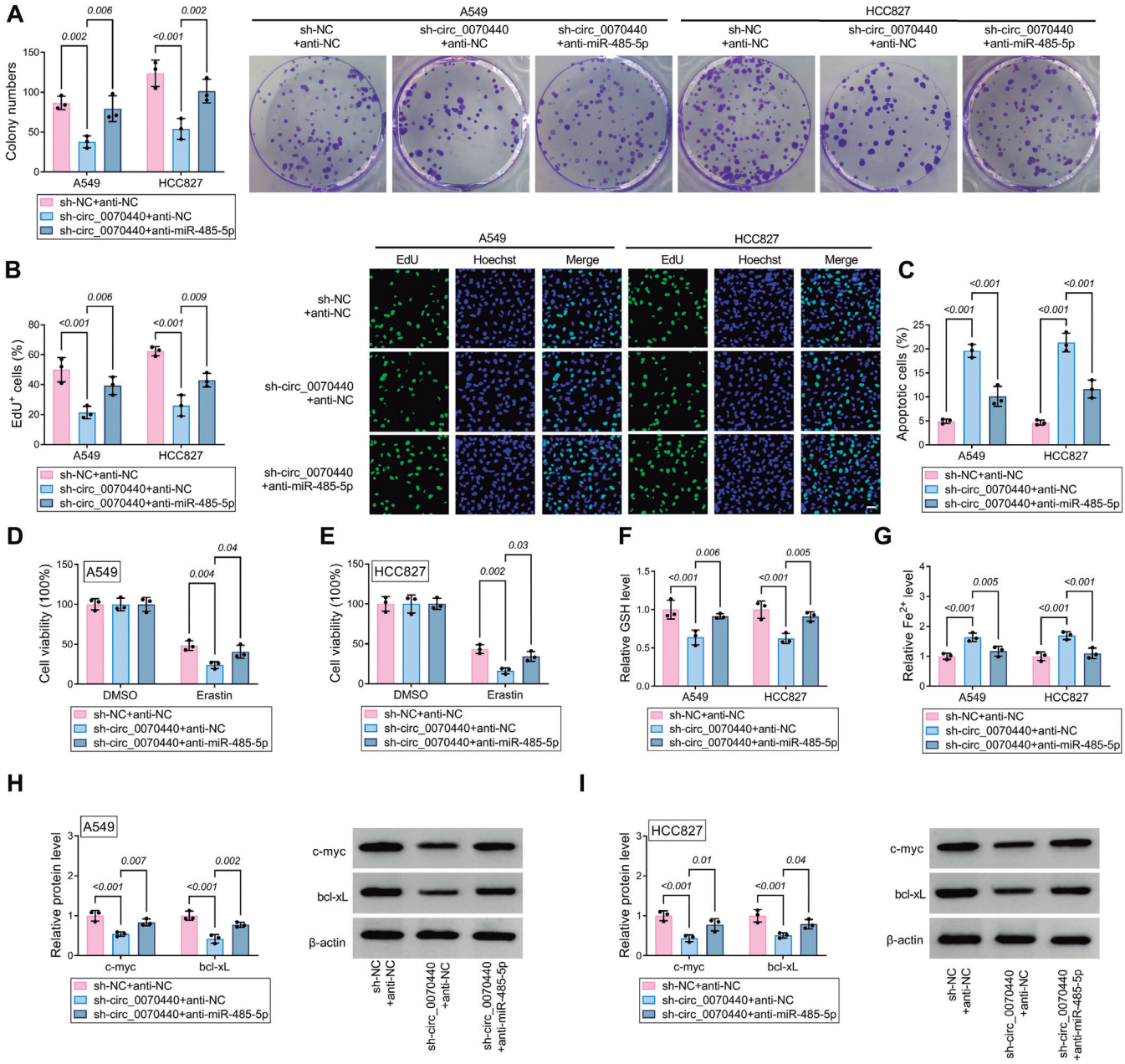

Fig. 6. Circ_0070440 facilitated cell progression by targeting miR-485-5p. **A, B.** Cell proliferation. **C.** Apoptosis. **D, E.** Cell viability of Erastin-treated. **F.** GSH level. **G.** Fe^{2+} level. **H, I.** protein levels of c-myc and bcl-xl were measured in A549 and HCC827 cells with circ_0070440 knockdown and miR-485-5p knockdown. Data represent mean±SD. Scale bars: 50 μm.

ferroptosis regulation (Zheng and Conrad, 2020; Zhi et al., 2021). For instance, miR-5096 can bind with SLC7A11-3' UTR to induce ferroptosis and retard tumorigenic properties in breast cancer (Yadav et al., 2021). ELAVL1-induced lncRNA LINC00336 acted as an oncogene by regulating the miR-6853/CBS pathway to constrain ferroptosis in lung cancer (Wang et al., 2019). Furthermore, circEPSTI1 inhibited ferroptosis and contributed to malignancy by sponging miR-375/409-3p/515-5p to increase the SLC7A11 level in cervical cancer (Wu et al., 2021). Nevertheless, few studies have manifested the crucial role of circRNA in ferroptosis-regulated LUAD.

In this study, a novel circRNA circ_0070440 was disclosed that was up-regulated in LUAD cells. Circ_0070440 originates from the back-splicing of exons 2 and 3 of the FAM13A gene, which is associated with pulmonary diseases, such as chronic obstructive pulmonary disease (Castaldi et al., 2019), pulmonary fibrosis (Yao et al., 2019), and lung cancer (Eisenhut et al., 2017). Previous results have shown that circRNA may positively regulate its parent gene (Zhou et al., 2019). We speculated that circ_0070440 may have some connection with FAM13A in LUAD. Disappointingly, our results suggested that circ_0070440 failed to regulate FAM13A expression. Here, the data showed that the knockdown of circ_0070440 in LUAD cells could effectively suppress proliferation and promote apoptosis, and tumor growth *in vitro* and *in vivo*. Moreover, circ_0070440 silencing intensified the Erastin-induced inhibitory effect of cell viability on LUAD cells. Loss of circ_0070440 also reduced the GSH level and increased the Fe^{2+} level. These data show that circ_0070440 regulated the new function of ferroptosis in the malignant progression of LUAD and provided worthy evidence for the key role of circRNA in the ferroptosis of LUAD cells. In future investigations, the correlation between circ_0070440-mediated apoptosis and ferroptosis should be confirmed.

Previous studies have manifested that SLC7A11 might act as a tumor promoter to participate in a ferroptosis-dependent or independent manner. For example, YTHDC2 was reduced in LUAD and impeded LUAD tumorigenesis by destabilizing SLC7A11 mRNA and SLC7A11-dependent antioxidant function in an m6A-dependent manner (Ji et al., 2018). Moreover, RBMS1 ablation hampered lung cancer development by reducing SLC7A11-mediated radioresistance and

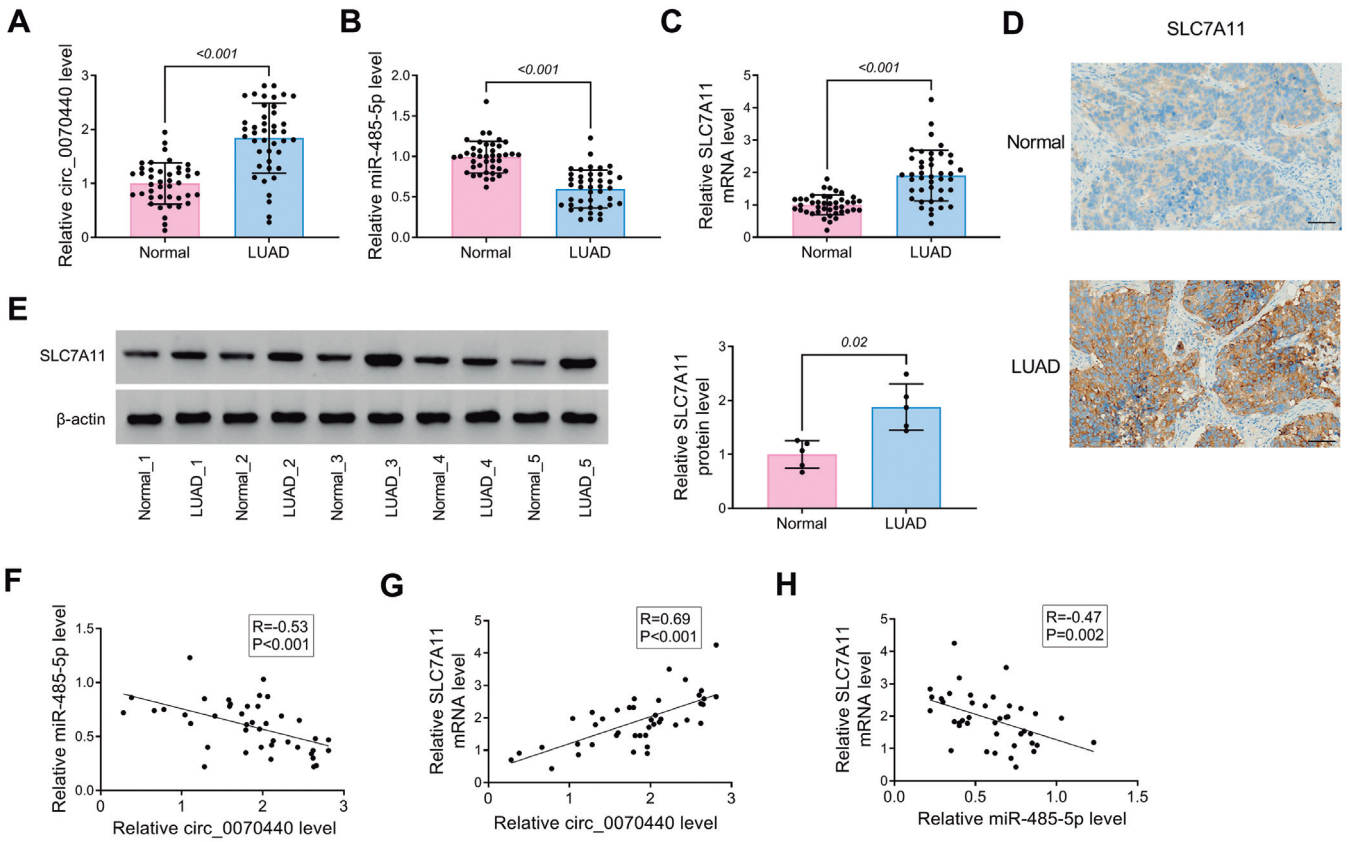

Fig. 7. Expression of circ_0070440, miR-485-5p, and SLC7A11 in LUAD tissues. **A-C.** Expression of circ_0070440, miR-485-5p, and SLC7A11 in 42 sets of paired LUAD and normal adjacent tissues (Normal). **D, E.** The protein level of SLC7A11 was tested by IHC and WB. **F-H.** Correlation between circ_0070440, miR-485-5p, and SLC7A11 expression in LUAD tissues. Data represent mean±SD. Scale bars: 100 μm.

inhibiting the effects of ferroptosis (Ma et al., 2021). We speculated that circ_0070440 may regulate SLC7A11-mediated LUAD development. Next, we detected the protein levels of SLC7A11 and its downstream molecules c-myc and bcl-xl (Zhang et al., 2021b). As expected, circ_0070440 ablation retarded the protein levels of SLC7A11, c-myc, and bcl-xl. Furthermore, the rescue experiments disclosed that ectopic SLC7A11 expression ameliorated the inhibitory effects on sh-circ_0070440-mediated LUAD cell proliferation, apoptosis, and ferroptosis.

Increasingly studies have revealed that miRNA was a key downstream regulatory factor in circRNA-mediated LUAD development. Circ-ENO1 impelled glucose metabolism and LUAD progression by interacting with miR-22-3p to elevate its host gene ENO1 level (Zhou et al., 2019). Hsa_circ_0000326 played a role in promoting LUAD by sponging miR-338-3p to augment RAB14-mediated proliferation, migration, and apoptosis (Xu et al., 2020). In this study, we speculated that circ_0070440 elevated the SLC7A11 level by sponging miR-485-5p. Previous investigations have implicated the anti-tumor function of miR-485-5p in multiple tumors, such as osteosarcoma(Ding et al., 2021) and hepatocellular carcinoma (Yang et al., 2022). MiR-485-5p also participated in the regulatory network of LUAD pathogenesis. MiR-485-5p inhibited LUAD cell growth and migration by blocking WLS expression (Li et al., 2020). Loss of miR-485-5p facilitated LUAD cell metastasis and EMT via targeting Flot2 and triggering the activity of the PI3K/AKT/mTOR pathway (Mou and Liu, 2016). However, the role of miR-485-5p in the ferroptosis of LUAD was still unknown. Our mechanistic investigation presented that circ_0070440 might enhance SLC7A11 expression by sponging miR-485-5p. Further rescue assays showed that anti-miR-485-5p reversed circ_0070440 depletion-inhibited proliferation and circ_0070440 depletion-increased apoptosis and ferroptosis of LUAD cells. These data disclosed an unreported mechanism of circ_0070440, miR-485-5p, and SLC7A11 in LUAD cell proliferation, apoptosis, and ferroptosis. Our results did not exclude those other molecules such as miRNAs or RNA-binding proteins involved in circ_0070440/SLC7A11 pathway-mediated LUAD progression.

We further studied the expression of circ_0070440, miR-485-5p, and SLC7A11 in LUAD and normal adjacent tissues. Circ_0070440 and SLC7A11 were highly expressed while miR-485-5p was weakly expressed in LUAD. In addition, there was a positive correlation between circ_0070440 and SLC7A11 levels, while both circ_0070440 and SLC7A11 levels were negatively correlated with miR-485-5p level, further indicating that the circ_0070440/miR-485-5p/SLC7A11 axis was related to LUAD progression.

In summary, circ_0070440 was up-regulated in LUAD and might serve as a sponge of miR-485-5p to promote SLC7A11-mediated ferroptosis-related phenotypes in LUAD cells. Additionally, the circ_0070440/miR-485-5p/SLC7A11 axis has indicated their potential as biomarkers for clinical detection in LUAD.

Acknowledgements. Not applicable.

Funding. No funding was received.

Ethics approval and consent to participate. The present study was approved by the ethical review committee of the Affiliated Hospital of Jiangnan University (South Branch). Written informed consent was obtained from all enrolled patients.

Consent for publication. Patients agree to participate in this work

Availability of data and materials. The analyzed data sets generated during the present study are available from the corresponding author on reasonable request.

Authors' contribution. Conceptualization and Methodology: Qichen Cui and Jian Shen; Formal analysis and Data curation: Jian Shen, Weihong Shen and Yuan Weng; Validation and Investigation: Yong Zhao, Qichen Cui and Jian Shen; Writing - original draft preparation and Writing - review and editing: Yong Zhao, Qichen Cui, Jian Shen and Weihong Shen; Approval of final manuscript: all authors

Competing interests. The authors declare that they have no competing interests.

References

Barta J.A., Powell C.A. and Wisnivesky J.P. (2019). Global epidemiology of lung cancer. Ann. Glob. Health 85, 8.

Bing H., Jie C. and Honghong Y. (2018). Circular RNA and its mechanisms in disease: From the bench to the clinic. Pharmacol. Ther. 187, 31-44.

Castaldi P.J., Guo F., Qiao D., Du F., Naing Z.Z.C., Li Y., Pham B., Mikkelsen T.S., Cho M.H., Silverman E.K. and Zhou X. (2019). Identification of functional variants in the FAM13A chronic obstructive pulmonary disease genome-wide association study locus by massively parallel reporter assays. Am. J. Respir. Crit. Care Med. 199, 52-61.

Chen R., Liu Y., Zhuang H., Yang B., Hei K., Xiao M., Hou C., Gao H., Zhang X., Jia C., Li L., Li Y. and Zhang N. (2017). Quantitative proteomics reveals that long non-coding RNA MALAT1 interacts with DBC1 to regulate p53 acetylation. Nucleic Acids Res. 45, 9947-9959.

Ding L., Liu T., Qu Y., Kang Z., Guo L., Zhang H., Jiang J., Qu F., Ge W. and Zhang S. (2021). LncRNA MELTF-AS1 facilitates osteosarcoma metastasis by modulating MMP14 expression. Mol. Ther. Nucleic Acids 26, 787-797.

Ebbesen K.K., Kjems J. and Hansen T.B. (2016). Circular RNAs: Identification, biogenesis and function. Biochim. Biophys. Acta 1859, 163-168.

Eisenhut F., Heim L., Trump S., Mittler S., Sopel N., Andreev K., Ferrazzi F., Ekici A.B., Rieker R., Springel R., Assmann V.L., Lechmann M., Koch S., Engelhardt M., Warnecke C., Trufa D.I., Sirbu H., Hartmann A. and Finotto S. (2017). FAM13A is associated with non-small cell lung cancer (NSCLC) progression and controls tumor cell proliferation and survival. Oncoimmunology 6, e1256526.

Hansen T.B., Jensen T.I., Clausen B.H., Bramsen J.B., Finsen B., Damgaard C.K. and Kjems J. (2013). Natural RNA circles function as efficient microRNA sponges. Nature 495, 384-388.

Hu K., Li K., Lv J., Feng J., Chen J., Wu H., Cheng F., Jiang W., Wang

J., Pei H., Chiao P.J., Cai Z., Chen Y., Liu M. and Pang X. (2020). Suppression of the SLC7A11/glutathione axis causes synthetic lethality in KRAS-mutant lung adenocarcinoma. J. Clin. Invest. 130, 1752-1766.

Ji X., Qian J., Rahman S.M.J., Siska P.J., Zou Y., Harris B.K., Hoeksema M.D., Trenary I.A., Heidi C., Eisenberg R., Rathmell J.C., Young J.D. and Massion P.P. (2018). xCT (SLC7A11)-mediated metabolic reprogramming promotes non-small cell lung cancer progression. Oncogene 37, 5007-5019.

Koppula P., Zhuang L. and Gan B. (2021). Cystine transporter SLC7A11/xCT in cancer: Ferroptosis, nutrient dependency, and cancer therapy. Protein Cell 12, 599-620.

Lambe G., Durand M., Buckley A., Nicholson S. and McDermott R. (2020). Adenocarcinoma of the lung: From BAC to the future. Insights Imaging 11, 69.

Li J.H., Liu S., Zhou H., Qu L.H. and Yang J.H. (2014). StarBase v2.0: Decoding miRNA-ceRNA, miRNA-ncRNA and protein-RNA interaction networks from large-scale CLIP-Seq data. Nucleic Acids Res. 42, D92-97.

Li W., Zheng Y., Mao B., Wang F., Zhong Y. and Cheng D. (2020). SNHG17 upregulates WLS expression to accelerate lung adenocarcinoma progression by sponging miR-485-5p. Biochem. Biophys. Res. Commun. 533, 1435-1441.

Liu M., Wang Q., Shen J., Yang B.B. and Ding X. (2019). Circbank: A comprehensive database for circRNA with standard nomenclature. RNA Biol. 16, 899-905.

Liu H., Lan T., Li H., Xu L., Chen X., Liao H., Chen X., Du J., Cai Y., Wang J., Li X., Huang J., Yuan K. and Zeng Y. (2021). Circular RNA circDLC1 inhibits MMP1-mediated liver cancer progression via interaction with HUR. Theranostics 11, 1396-1411.

Ma L., Chen T., Zhang X., Miao Y., Tian X., Yu K., Xu X., Niu Y., Guo S., Zhang C., Qiu S., Qiao Y., Fang W., Du L., Yu Y. and Wang J. (2021). The m6A reader YTHDC2 inhibits lung adenocarcinoma tumorigenesis by suppressing SLC7A11-dependent antioxidant function. Redox Biol. 38, 101801-101801.

Mao W., Wang K., Xu B., Zhang H., Sun S., Hu Q., Zhang L., Liu C., Chen S., Wu J., Chen M., Li W. and Peng B. (2021). CiRS-7 is a prognostic biomarker and potential gene therapy target for renal cell carcinoma. Mol. Cancer 20, 142.

Mou X. and Liu S. (2016). MiR-485 inhibits metastasis and EMT of lung adenocarcinoma by targeting Flot2. Biochem. Biophys. Res. Commun. 477, 521-526.

Succony L., Rassl D.M., Barker A.P., McCaughan F.M. and Rintoul R.C. (2021). Adenocarcinoma spectrum lesions of the lung: Detection, pathology and treatment strategies. Cancer Treat. Rev. 99, 102237.

Sung H., Ferlay J., Siegel R.L., Laversanne M., Soerjomataram I., Jemal A. and Bray F. (2021). Global cancer statistics 2020: GLOBOCAN estimates of incidence and mortality worldwide for 36 cancers in 185 countries. CA Cancer J. Clin. 71, 209-249.

Tao M., Zheng M., Xu Y., Ma S., Zhang W. and Ju S. (2021). CircRNAs and their regulatory roles in cancers. Mol. Med. 27, 94.

Wang M., Mao C., Ouyang L., Liu Y., Lai W., Liu N., Shi Y., Chen L., Xiao D., Yu F., Wang X., Zhou H., Cao Y., Liu S., Yan Q., Tao Y. and Zhang B. (2019). Long noncoding RNA LINC00336 inhibits ferroptosis in lung cancer by functioning as a competing endogenous RNA. Cell Death Differ. 26, 2329-2343.

Wu P., Li C., Ye D.M., Yu K., Li Y., Tang H., Xu G., Yi S. and Zhang Z. (2021). Circular RNA circEPTI1 accelerates cervical cancer progression via miR-375/409-3p/515-5p-SLC7A11 axis. Aging (Albany NY) 13, 4663-4673.

Xu Y., Yu J., Huang Z., Fu B., Tao Y., Qi X., Mou Y., Hu Y., Wang Y., Cao Y., Jiang D., Xie J., Xu Y., Zhao J. and Xiong W. (2020). Circular RNA hsa_circ_0000326 acts as a mir-338-3p sponge to facilitate lung adenocarcinoma progression. J. Exp. Clin. Cancer Res. 39, 57.

Yadav P., Sharma P., Sundaram S., Venkatraman G., Bera A.K. and Karunagaran D. (2021). SLC7A11/ xCT is a target of miR-5096 and its restoration partially rescues miR-5096-mediated ferroptosis and anti-tumor effects in human breast cancer cells. Cancer Lett. 522, 211-224.

Yang L., Deng W.-L., Zhao B.-G., Xu Y., Wang X.-W., Fang Y. and Xiao H.-J. (2022). FOXO3-induced lncRNA LOC554202 contributes to hepatocellular carcinoma progression via the miR-485-5p/BSG axis. Cancer Gene Ther. 29, 326-340.

Yao M.-Y., Zhang W.-H., Ma W.-T., Liu Q.-H., Xing L.-H. and Zhao G.-F. (2019). MicroRNA-328 in exosomes derived from M2 macrophages exerts a promotive effect on the progression of pulmonary fibrosis via FAM13A in a rat model. Exp. Mol. Med. 51, 1-16.

Yuan B., Liao F., Shi Z.-Z., Ren Y., Deng X.-L., Yang T.-T., Li D.-Y., Li R.-F., Pu D.-D., Wang Y.-J., Tan Y., Yang Z. and Zhang Y.-H. (2020). Dihydroartemisinin inhibits the proliferation, colony formation and induces ferroptosis of lung cancer cells by inhibiting PRIM2/SLC7A11 axis. Onco. Targets Ther. 13, 10829-10840.

Zhang N., Nan A., Chen L., Li X., Jia Y., Qiu M., Dai X., Zhou H., Zhu J., Zhang H. and Jiang Y. (2020). Circular RNA circSATB2 promotes progression of non-small cell lung cancer cells. Mol. Cancer 19, 101.

Zhang H., Ge Z., Wang Z., Gao Y., Wang Y. and Qu X. (2021a). Circular RNA RHOT1 promotes progression and inhibits ferroptosis via mir-106a-5p/STAT3 axis in breast cancer. Aging (Albany NY) 13, 8115-8126.

Zhang W., Sun Y., Bai L., Zhi L., Yang Y., Zhao Q., Chen C., Qi Y., Gao W., He W., Wang L., Chen D., Fan S., Chen H., Piao H.-L., Qiao Q., Xu Z., Zhang J., Zhao J., Zhang S., Yin Y., Peng C., Li X., Liu Q., Liu H. and Wang Y. (2021b). RBMS1 regulates lung cancer ferroptosis through translational control of SLC7A11. J. Clin. Invest 131, E152067.

Zheng J. and Conrad M. (2020). The metabolic underpinnings of ferroptosis. Cell Metab. 32, 920-937.

Zhi Y., Gao L., Wang B., Ren W., Liang K.X. and Zhi K. (2021). Ferroptosis holds novel promise in treatment of cancer mediated by non-coding RNAs. Front. Cell Dev. Biol. 9, 686906.

Zhou J., Zhang S., Chen Z., He Z., Xu Y. and Li Z. (2019). CircRNA-ENO1 promoted glycolysis and tumor progression in lung adenocarcinoma through upregulating its host gene ENO1. Cell Death Dis. 10, 885.

Zhou Q.-Y., Gui S.-Y., Zhang P. and Wang M. (2021). Upregulation of miR-345-5p suppresses cell growth of lung adenocarcinoma by regulating ras homolog family member A (RhoA) and Rho/Rho associated protein kinase (Rho/ROCK) pathway. Chin. Med. J. (Engl) 134, 2619-2628.

Accepted February 22, 2023